

Chapter 11

Remote Sensing of Terrestrial Water



Kazuyoshi Suzuki and Koji Matsuo

11.1 Introduction

Terrestrial water (TW) is a critical component of ecosystems and is important for hydroclimatology and human usage. As described by Suzuki (2011), the considerable snow and ice coverage in eastern Siberia are essential components in estimating the amount of terrestrial water in the region (both in liquid and frozen state). With regard to the role of terrestrial water in ecosystems in eastern Siberia, Sugimoto et al. (2003) showed that soil moisture (SM) acts as a reservoir for plant growth when summer precipitation is insufficient. In addition, Suzuki et al. (2006) demonstrated that SM and snow water equivalent in the fall affect runoff from snowmelt in the following year. Having said this, terrestrial water is an important resource for people living in eastern Siberia, and thus, the security of terrestrial water is crucial (Dudarev et al. 2013). According to Suzuki (2011), the depth of permafrost is more than 100 m. Thus, locals in eastern Siberia find the groundwater located at greater depths difficult to use. In this chapter, we explain the manner in which recently developed remote sensing techniques are used to quantify terrestrial water and review the available datasets and previously obtained research results in eastern Siberia. The region is predominantly covered by the taiga forest, which is dominated by species such as larch. The forest cover hinders the detection of TW from space; the effects of the forest and other vegetation cover on remote sensing-based retrievals of terrestrial water must be considered. Terrestrial water is equivalent to terrestrial water storage (TWS), which includes all of water stored on land, such as SM, snow, surface water (SW), and ice in the permafrost. However, we have ignored the glaciers in eastern Siberia because they are relatively smaller in size (Earl and Gardner 2016). We have also ignored the water

K. Suzuki (✉)

Japan Agency for Marine-Earth Science and Technology, Yokohama, Japan
e-mail: skazu@jamstec.go.jp

K. Matsuo

The Geospatial Information Authority of Japan, Tsukuba, Japan

present below the permafrost because the depth of permafrost is too deep, and the water can be isolated from the terrestrial water cycle system. Therefore, the current chapter will focus on SM, snow, and SW. Ice in permafrost are included in the TWS anomaly estimates covering eastern Siberia. We have addressed those changes using TWS anomalies assessed using satellite remote sensing.

In Sect. 11.2 of this chapter, we describe remote sensing-based techniques for assessing TWS. In Sects. 11.3, 11.4, and 11.5, we then describe remote sensing-based techniques for assessing different components of TWS, specifically SM, snow, and SW, respectively, in eastern Siberia. Section 11.6 discusses recent advancements in data assimilation techniques using remote sensing data. Since remote sensing data are only available over limited geographic and temporal ranges, they must be merged with other sources of information to generate spatially and temporally consistent datasets. Each section contains several subsections, including an outline, a description of the available datasets, results of previous studies, and a perspective. Finally, in Sect. 11.7, we provide concluding remarks and research perspectives for the near future.

11.2 Terrestrial Water Storage (TWS)

This section describes remote sensing methods for estimating TWS and their scientific applications in eastern Siberia. It is difficult to directly assess the actual TWS from space, but it has recently become possible to measure TWS anomalies from space using satellite gravimetric observations.

11.2.1 Remote Sensing of TWS

Masuda et al. (2001) assessed the seasonal characteristics of TWS in large rivers worldwide using river runoff and reanalysis datasets. However, the interannual variations in TWS cannot be estimated by this method because the climatological TWS was derived only as the residual term of the atmospheric water balance. To determine monthly changes in TWS, alternative methods are required.

The measurements of TWS anomalies from space have been available since 2002 and are based on data obtained from gravity observation satellite missions, such as the Gravity Recovery And Climate Experiment (GRACE) (Wahr et al. 1998). GRACE uses twin satellites that are separated by approximately 220 km and follow the same orbital path and altitude in a near-polar orbit at approximately 500 km above the Earth. A precise microwave distance-measuring device (K-band ranging, KBR) with two frequencies (24-GHz K-band and 32 GHz Ka-band) is on board both satellites and is used to measure changes in the distance between the twin satellites. This instrument is extremely sensitive, enabling the measurement of changes in the inter-satellite distance to an accuracy of 1 μm .

One of the major goals of the GRACE mission is to perform high-precision measurements of the Earth's static gravity field. In the same way, the mission is also intended to observe the dynamics of the Earth's gravity field (i.e., the time-variable gravity field). GRACE can measure the Earth's gravity field to an accuracy of several μGal (i.e., hundreds of millionths of Earth standard gravity) with spatial and temporal resolutions of a few hundred kilometers and a month, respectively. By observing gravity, we can directly estimate mass changes, such as those associated with precipitation, evaporation, and river runoff. In this article, we describe the observations of mass changes related to climate change.

Seasonal gravity changes over continental areas mainly reflect changes in the soil water content caused primarily due to rainfall and snowfall (Tapley et al. 2004). Conspicuous gravity changes are observed in low-latitude areas (from 30°N to 30°S), particularly in South America, Africa, northern Australia, and southeastern Asia. The gravity force in these areas increases in summer through autumn and decreases in winter through spring; this closely corresponds to the temporal rainfall pattern of the tropical monsoon climate. Conspicuous gravity changes are also seen in the high-latitude regions of the Northern Hemisphere (from 45°N to 75°N). The gravity force there increases in winter through spring and decreases in summer through autumn; it parallels the temporal patterns of rainfall and snowfall seen in the damp climate of the subarctic zone.

11.2.2 TWS Datasets

GRACE data processing is conducted at various analysis centers, and changes in the inter-satellite distance are converted to gravity data. There are three main analysis centers: the Center for Space Research (CSR) at the University of Texas, the Jet Propulsion Laboratory (JPL) of the National Aeronautics and Space Administration (NASA), and the GeoForschungsZentrum (GFZ) in Potsdam, Germany. In addition, the Center National d'Etudes Spatiales (CNES) and the Delft University of Technology (DMT), as well as other centers, have also developed original analytic solutions. The products of the first processing step that is applied to the measured inter-satellite distance changes are called the Level-1B data. A second treatment is then performed to convert the data to spherical harmonic coefficients (also called Stokes coefficients) of the change in the gravitational potential over the entire Earth, which are called the Level-2 data. In this step, various geophysical corrections, such as corrections for tidal effects, atmospheric and oceanic effects, and non-gravitational accelerations, are applied (e.g., Bettadpur 2012). Using the Level-2 data, we can estimate TWS anomalies using the following steps: (1) corrections for postglacial rebound (PGR) or glacial isostatic adjustment (GIA) are made using geophysical models (e.g., Geruo et al. 2013); (2) a filter (specifically a Gaussian or stochastic filter) is applied to remove north-south striping noises and high-frequency noises (Kusche 2007); (3) the changes in the degree-1 components of the Earth's gravity field (the center of mass of the Earth) are accounted for via

reanalysis output, using the methods described by Swenson and Wahr (2006); (4) the change in equivalent water thickness (EWT) is estimated using the methods described by Wahr et al. (1998); and (5) the uncertainties in EWT are estimated using error variance matrices of GRACE observations (Wahr et al. 2004).

The GRACE EWT products, after the abovementioned data processing, are termed Level-3 data. These data are available for download from the Internet [e.g., from NASA JPL (<ftp://podaac-ftp.jpl.nasa.gov/allData/grace>)]. The Level-3 data are represented on a grid that expands up to a degree and order 60 in terms of spherical harmonics. The Level-2 data are also available in the form of the spherical harmonic coefficients up to degree and order 96, but the effective spatial resolution is approximately 300 km. Data covering the period from April 2002 to June 2017 are available from the following three websites:

The GRACE Tellus website (<http://grace.jpl.nasa.gov/>) provides maps of surface mass anomalies. This site also provides products created synergistically with GRACE and TOPEX (TOPOgraphy EXperiment) /Jason-1 missions (a joint satellite mission between NASA, the US space agency, and CNES, the French space agency, to map ocean surface topography). The CU GRACE website (<http://geoid.colorado.edu/>) provides mass anomalies in regional or global time series. The NASA GRACE website (<https://podaac.jpl.nasa.gov/>) provides the GRACE Level-1B and Level-2 products. The GFZ GRACE website (<http://isdc.gfz-potsdam.de/grace-isdc/>) provides the GRACE Level-1B and Level-2 products. The ICGEM website (<http://icgem.gfz-potsdam.de/ICGEM/ICGEM.html>) distributes a full range of current and historical static Earth gravity field models.

11.2.3 *Scientific Applications of TWS*

We will first explain the manner in which GRACE-based TWS has been used in estimating the wetting and drying of terrestrial land in recent years and the linkage between TWS and river runoff in eastern Siberia.

The Lena River basin is the second-largest source of freshwater inflow into the Arctic Ocean. Hydrological studies conducted in cold regions have shown that TWS strongly affects the amount of river flow from basins (Quinton et al. 2003; Papa et al. 2008; Hood and Hayashi 2015). Therefore, it is important to evaluate the variability of TWS. Muskett and Romanovsky (2009) and Velicogna et al. (2012) reported that GRACE data showed increased TWS throughout the Lena River basin from 2002 to 2010 primarily because of rising groundwater levels in the discontinuous permafrost zone. In contrast, Vey et al. (2013) noted that such an increasing trend in TWS was cancelled by a decreasing trend in TWS, after 2009, in the Lena River basin. Suzuki et al. (2016) used 146 months of data from GRACE spanning April 2002 to August 2015 to analyze TWS in the Lena River basin. A negative trend in TWS in the downstream reaches of the Lena River basin was primarily due to evapotranspiration. The coefficient of determination indicates that 37% of the variance in regional TWS can be explained by a linear function of evapotranspiration. In turn, summer air

temperatures control evapotranspiration, which mostly occurs from June to August. Further warming during summer at high latitudes in the Lena River basin might enhance the already-substantial reduction in TWS in the area.

Next, we will present basin-scale TWS changes in the Lena River basin. Figure 11.1(a) shows the temporal variations in the basin-averaged monthly TWS anomalies determined by GRACE and GLDAS (Global Land Data Assimilation System). The GRACE- and GLDAS-based TWS (TWS_{GRACE} and TWS_{GLDAS}) results are highly correlated ($r = 0.71$, $p < 0.0001$). The correlation coefficient “ r ” indicates the strength of the linear relationship between TWS_{GRACE} and TWS_{GLDAS} ; the coefficient of determination R^2 indicates the degree to which the variance can be explained by a linear model. Based on the high degree of correlation between the two TWS datasets, we were able to calculate a basin-scale TWS change of approximately 50% using GLDAS, thus allowing us to determine the primary factor controlling the changes in TWS_{GRACE} . The similarity between the two datasets implied that both TWS_{GLDAS} and TWS_{GRACE} depend largely on snow water equivalent (SWE) and SM.

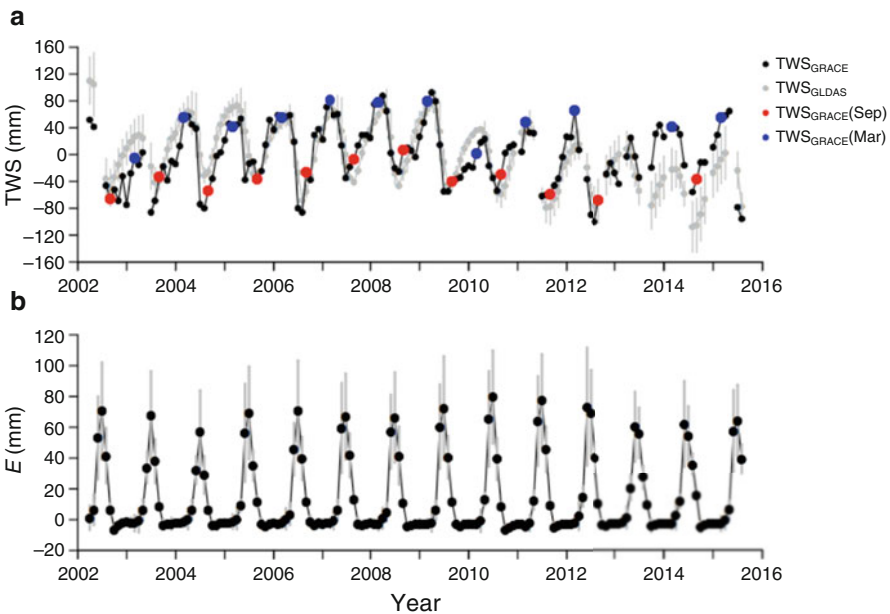


Fig. 11.1 (a) Temporal variations in TWS in the Lena River basin. Black and gray circles indicate TWS_{GRACE} and TWS_{GLDAS} data, respectively, and red and blue circles indicate GRACE-based TWS estimates in September ($TWS_{GRACE(Sep)}$) and March ($TWS_{GRACE(Mar)}$), respectively. Vertical gray bars indicate the standard deviation of the multi-model GLDAS ensemble. (b) Temporal variations in the monthly evapotranspiration (E), shown with the standard deviation of the multi-model GLDAS ensemble. Reproduced from Fig. 2 in (Suzuki et al. 2016)

As reported previously (Vey et al. 2013), the basin-averaged TWS_{GRACE} shown in Fig. 11.1(a) does not exhibit any clear trend because of the decrease in TWS after 2009. To explain this apparent lack of trend in TWS_{GRACE} , we examined monthly basin-averaged evapotranspiration [Fig. 11.1(b)]. Evapotranspiration from June to August 2009 was more than 12 mm greater than the 14-year average and more than 20 mm greater during the following 3 years. Consistent with these higher evapotranspiration levels, TWS_{GRACE} in September decreased steadily from 2010 to 2012. This finding suggests that the increased summer evapotranspiration from 2009 to 2012 caused a decrease in TWS in the Lena River basin beginning in 2010. The TWS did not exhibit an overall trend from 2002 to 2015, as shown in Fig. 11.1(a).

Next, we will demonstrate another example of research using GRACE-based TWS because these data are useful for understanding SW storage and river runoff as well as vegetation and solid precipitation in eastern Siberia.

The GRACE-based TWS data were used to understand changes in air temperature and the normalized difference vegetation index (NDVI). NDVI is commonly used as an index of vegetation activity. The relationship between NDVI and the 2-m air temperature (T_a) due to changes in TWS was investigated (Geruo et al. 2015). A strong correlation between NDVI and T_a was found for the Viluy River basin, which lies within the Lena River basin, but the NDVI values over the remainder of the Lena River basin were controlled by water availability (i.e., the NDVI–TWS relationship). During 2002 to 2011, wetter conditions in the Lena River basin were associated with increased NDVI. In these studies, the water from snowmelt was also an important controlling factor for early spring NDVI.

Solid precipitation is a dominant component of the hydrological cycle during winter. However, weather stations and observation networks are sparse in eastern Siberia. Therefore, space-based remote sensing techniques are useful for measuring solid precipitation in this region. Seo et al. (2010) estimated winter precipitation using GRACE-based TWS and snow data obtained using the Advanced Microwave Scanning Radiometer–Earth Observing System (AMSR-E). The authors found that the pattern of solid precipitation during winter derived from GRACE-based TWS is better than that derived from the AMSR-E snow product, when both datasets were compared with independent precipitation products. Specifically, the following products were used for comparison: the Global Precipitation Climatology Project (GPCP), the Climate Prediction Center’s Merged Analysis of Precipitation (CMAP), and three reanalysis data products, namely, the National Centers for Environmental Prediction/National Center for Atmospheric Research (NCEP/NCAR) reanalysis, the European Center for Medium-Range Weather Forecasts’ ERA-Interim reanalysis, and the Japan Meteorological Agency’s Climate Data Assimilation System (JCDAS) reanalysis. Among these estimates, the AMSR-E estimates differ the most from the other estimates; this indicates a possible large uncertainty in the AMSR-E-based estimates that might be caused by the physical properties of snowpack and the underlying surface and forest parameterization assumed in the current AMSR-E SWE algorithm. Therefore, using GRACE-based TWS is reliable for estimating winter

precipitation in eastern Siberia. However, the spatial and temporal resolutions of such winter precipitation estimates are very low.

The Arctic freshwater budget is critical for understanding the climate in the northern regions. However, the hydrology of the Arctic circumpolar tundra region and the largest pan-Arctic rivers are still not well understood. Suzuki et al. (2018) analyzed the spatiotemporal variations in the TWS of the Arctic circumpolar tundra region, including three of its largest pan-Arctic river basins (Lena, Mackenzie, and Yukon), using monthly GRACE data from 2002 to 2016. Together with global land reanalysis, and river runoff, they identified declining TWS trends throughout the Arctic circumpolar tundra region that we attributed largely to increasing evapotranspiration driven by increasing summer air temperatures. At the basin scale, Suzuki et al. (2018) showed that, in the Lena River basin, the autumnal TWS signal persisted until the winter of the following year, while in the Mackenzie River basin, TWS levels during autumn and winter showed no significant impact in the following year. This disparity may be due to differences in the continuous permafrost distribution between the two river basins. Since global warming is expected to be particularly significant in the northern regions, these results are important for understanding future TWS trends, as further declines are possible given the fact that Arctic temperatures continue to rise.

11.2.4 Perspectives on TWS Remote Sensing

Information on TWS is critical because it is both a component of the hydrological cycle and climate system and a key resource. GRACE has provided considerable advances in scientific knowledge in those areas. The power supply of the measuring instrument had been ensured by suspending measurements for approximately 1 month in every 6 months, beginning in 2011, to extend the practical use of the satellites; the useful lifetime of GRACE satellites ended in November 2017.

Therefore, a follow-on satellite mission is clearly needed and was planned by NASA and German Research Centre for Geosciences. The NASA/German Research Centre for Geosciences' Gravity Recovery and Climate Experiment Follow-On (GRACE-FO) spacecraft was successfully launched in May 2018; GRACE-FO plans to extend and improve its first GRACE mission. Though the resolution will be the same as GRACE (approximately 300 km), the accuracy could be improved by inter-satellite laser ranging system. The resulting data will foster major breakthroughs in several branches of the Earth sciences. For instance, GRACE-FO will offer details on the movement of water on the planet. In addition, GRACE-FO will provide more detailed TWS data in eastern Siberia, which will improve the understanding of regional water movement under climate change.

Given the availability of TWS data, the analysis of the relationship between river runoff and TWS anomalies was limited. Further improvements in our understanding of the Arctic freshwater cycle will require additional GRACE-based TWS estimates.

11.3 Soil Moisture (SM)

TWS includes deeper groundwater and snow, as well as SM; however, vegetation is largely dependent on surface SM. To assess soil evaporation and transpiration from vegetation in eastern Siberia, SM must be estimated. Estimating SM near the surface is important for understanding the partitioning of energy and water between the land and atmosphere as well as the cycling of carbon and other materials through life cycles of vegetation or the wetness of the surface soil layer. Therefore, many efforts have been made to retrieve SM from space. In this section, we review recently developed remote sensing techniques for performing SM retrievals.

11.3.1 Remote Sensing of SM

Optical remote sensing techniques have been used to measure proxies for SM, such as surface albedo and surface temperature, from space. However, these sensors cannot detect areas with cloud or vegetation cover.

Microwave remote sensing techniques are not obstructed by clouds. Moreover, these sensors can measure the dielectric constant of soil, which is related to water content. In addition, microwave sensors are useful even at night, when solar radiation is not available. Microwave remote sensing techniques are widely used to retrieve SM from space. The Institute of Electrical and Electronics Engineers (IEEE) has defined an IEEE Standard 521–1984, a system of electromagnetic frequency bands used for radio and radar. Microwaves comprise the L-band, which has a frequency range from 1 to 2 GHz, which corresponds to wavelengths of 30 cm to 15 cm; S-band, which has a frequency range of 2–4 GHz (wavelengths 15–5 cm); C-band with a frequency range of 4–8 GHz (wavelengths 5–3.75 cm); X-band, ranging from 8 to 12 GHz (wavelengths 3.75–2.5 cm); Ku-band, ranging from 12 to 18 GHz (wavelengths 2.5–1.6 cm); K-band, ranging from 18 to 26 GHz (wavelengths 1.6–1.2 cm); Ka-band, ranging from 26 to 40 GHz (wavelengths 1.2 cm to 750 mm); V-band, ranging from 40 to 75 GHz (wavelengths 750–40 mm); and W-band, ranging from 75 to 111 GHz (wavelengths 40 mm to 28 mm). Estimates of SM from microwave information commonly use the L and C bands, which are unaffected by atmospheric conditions.

There are two types of microwave techniques involving either active or passive microwave sensors. Active microwave techniques provide fine spatial resolution but coarse temporal resolution; for example, scatterometers typically have a temporal resolution of 30 days but a spatial resolution of $0.1^\circ \times 0.1^\circ$. In contrast, passive microwave techniques offer coarse spatial resolution but high temporal resolution; for example, radiometers typically have a temporal resolution of 1–3 days but a spatial resolution of $38 \text{ km} \times 38 \text{ km}$.

In this section, we will describe the recently developed microwave remote sensing products and some research results obtained using those products in eastern Siberia.

11.3.2 SM Datasets

Table 11.1 shows the list of available SM datasets presented by Petropoulos et al. (2015). Researchers who require high-resolution data for specific purposes may wish to consider using the PALSAR (Phased Array type L-band Synthetic Aperture Radar) and ERS (Earth Resources Satellite) data, but the SM index must be retrieved from the original data provided by such sensors. The spatial resolution of these data is very fine (approximately 10 m), whereas their measurement interval is comparatively long at 10 days or much longer.

Here, we discuss the properties of each dataset presented in Table 11.1. The microwave frequencies that can be used to measure microwaves from the Earth's surface through the atmosphere include the L-band and C-band.

We introduce the operational SM analyses that are listed in Table 11.1.

Table 11.1 Operational soil moisture products produced using remote sensing techniques

	ASCAT	AMSR2	SMOS	SMAP
Instrument type	C-band (5.255 GHz) (Advanced Scatterometer)	Eight channels from 6.93 to 89.0 GHz (Advanced Microwave Scanning Radiometer-2)	L-band (1.4 GHz) (L-band radiometer)	L-band (1.2–1.4 GHz) (an L-band radar and an L-band radiometer) Note: The L-band radar stopped working on July 7, 2015
Temporal coverage	Since 2007	Since 2012	Since 2010	Since 2015
Spatial resolution	25 km	25 km, 50 km	35 km	40 km
Temporal resolution	3 days	0.5 days	1–3 days	3 days
References	Figa-Saldaña et al. (2002), Wagner et al. (2013)	Kachi et al. (2015)	Kerr et al. (2010)	Entekhabi et al. (2010)
Distributed by	European Organization for the Exploitation of Meteorological Satellites (EUMETSAT)	Japan Aerospace Exploration Agency (JAXA)	European Space Agency (ESA)	National Aeronautics and Space Administration (NASA)
Download portal	http://www.remss.com/missions/ascat	https://gcom-w1.jaxa.jp/auth.html	https://smos-ds-02.eo.esa.int/oads/access/	https://smap.jpl.nasa.gov/data/

11.3.2.1 ASCAT

This SM dataset is based on radar backscatter measurements within the C-band recorded by the Advanced Scatterometer (ASCAT) instrument aboard the EUMETSAT MetOp satellite. These data are first normalized to a common incidence angle (40°) using a radar backscatter model. The physical basis for the capability of ASCAT to measure SM is the strong dependence of C-band backscatter on the SM content in the topsoil layer (usually held to be 1–2 cm thick). The algorithm for the ASCAT SM product was developed by the Vienna University of Technology (TU Wien) and was designed to be a change detection method. The obtained radar backscatter coefficient is a function of the SM: low values correspond to a low SM, whereas high values are associated with a high SM. Radar backscatter values are scaled between 0% (dry soil) and 100% (wet soil that is saturated with water). The backscatter values are affected by soil texture and roughness. Thus, it is important to minimize those effects on SM estimation.

The surface SM content m_s is estimated in one of the last processing steps using:

$$m_s = \frac{\sigma^\circ - \sigma_{\text{dry}}^\circ}{\sigma_{\text{wet}}^\circ - \sigma_{\text{dry}}^\circ} \quad (11.1)$$

where σ° is the backscatter measurement to be inverted and $\sigma_{\text{dry}}^\circ$ and $\sigma_{\text{wet}}^\circ$ are the backscattering measurements representing dry and wet earth, respectively. For cold regions, the validation for ASCAT SM products was carried out at the Naqu site on the Tibetan Plateau.

11.3.2.2 AMSR2

The AMSR2 instrument, which is onboard the first-generation Global Change Observation Mission-Water (GCOM-W1) satellite, is a multifrequency, total-power microwave radiometer system with dual polarization channels for all frequency bands (Imaoka et al. 2010; Kachi et al. 2015). This sensor is a successor to the AMSR sensor that is on board the Advanced Earth Observing Satellite-II (ADEOS-II) and AMSR-E onboard NASA's Aqua satellite. The GCOM-W1 satellite was launched from the Japan Aerospace Exploration Agency (JAXA) on May 18, 2012 (JST), and was placed in orbit in front of the Aqua satellite. This was done to provide continuity with the AMSR-E observations (from June 2002 to October 2011) and provide synergy with the other instruments on A-Train (a satellite constellation, a string of meteorological and environmental Earth observation) satellites. JAXA releases AMSR2 geophysical parameters to the public through the GCOM-W1 data providing service system (<https://gcom-w1.jaxa.jp>). The validation for AMSR2 SM products was carried out in Mongolia.

11.3.2.3 SMOS

Another SM operational product that has become available more recently is based on data from the Soil Moisture and Ocean Salinity (SMOS) mission. SMOS was designed to measure SM over continental surfaces as well as ocean salinity using the low-microwave frequency (1.4 GHz) Microwave Imaging Radiometer with Aperture Synthesis (MIRAS) instrument. As of the beginning of October 2010, SMOS SM products were distributed to all relevant researchers. The SM products provide not only SM retrievals but also a series of ancillary data derived from the processing, namely, nadir optical thickness, surface temperature, and roughness parameter (namely, dielectric constant and brightness temperature retrieved at top of atmosphere and on the surface) with their corresponding uncertainties. For cold regions, the validation for SMOS SM products was carried out at the Naqu site on the Tibetan Plateau, China.

11.3.2.4 SMAP

The SMAP measurement approach is to integrate an L-band radar and an L-band radiometer as a single observation system, thereby combining the relative strengths of active and passive remote sensing for enhanced SM mapping. It was intended that the radar and radiometer measurements could be effectively combined to derive SM maps that approach the accuracy of radiometer-only retrievals. However, the radar measurements ceased 3 months after the launch (July 7, 2015), and, as of today, only the L-band radiometer remains functional. Since the effects of vegetation and surface roughness are dependent on incidence angle, the SMAP mission adopted a conical scan, constant incidence angle approach. This approach reduces the retrieval complexity and facilitates the use of time series retrieval algorithms. A 40° incidence angle was adopted for SMAP as a suitable angle for both radiometer and radar designs. The wide swath that results from this approach enables SMAP observations to provide global coverage in 2–3 days. For cold regions, the validation for the SMAP SM product was carried out in Manitoba and Winnipeg, Canada.

11.3.2.5 Land Parameter Retrieval Model (LPRM)

In addition to the datasets listed in Table 11.1, a useful historical climatology of continuous satellite-derived global land surface SM has been developed using the LPRM (Owe et al. 2008). The data consist of surface SM retrievals derived from all available historical and active satellite microwave sensors, including the Nimbus-7 Scanning Multichannel Microwave Radiometer, Defense Meteorological Satellites Program Special Sensor Microwave Imager, Tropical Rainfall Measuring Mission Microwave Imager, and Aqua Advanced Microwave Scanning Radiometer for Earth

Observing System, and span the period from November 1978 to the end of 2007. The validation for the LPRM SM product was carried out against other SM retrievals, such as ASCAT and SMOS.

11.3.3 Scientific Applications of SM

Eastern Siberia is mainly covered by forest, and thus, retrieving SM from satellite-based remote sensing measurements is challenging in this region as the forest canopy obscures the signal from water within the soil. Consequently, few studies have examined the application of SM retrieval data for this area.

Bartsch et al. (2009) showed that SM anomalies obtained using active microwave data are related to forest fire occurrence in Central Siberia. The authors showed an analysis of satellite-derived SM anomaly data from ERS-1/2 (ERS: Earth Resources Satellite) scatterometer data and burned area maps from MODIS/AVHRR/ATSR (Moderate Resolution Imaging Spectroradiometer/Advanced Very High-Resolution Radiometer/Along-Track Scanning Radiometer) over Central Siberia for the years 1992–2000. The results showed that wet surface SM conditions limit the extent of burned area and can prevent the outbreak of fires. Approximately 80% of all events occurred under drier conditions in July; the fire area was below 50 km² under moist conditions. Larger burned areas have not generally been detected when the surface wetness deviation exceeded +5%. Monitoring surface SM in Siberia will contribute to predicting forest fires in the region in the near future.

Current satellite remote sensing data products that include estimates of SM are limited to the surface soil layer extending to a depth of 5 cm. Estimating SM at greater depths is also important for understanding vegetation growth and water and carbon absorption in eastern Siberia. Van der Molen et al. (2016) evaluated whether the assimilation improved SiBCASA's SM and its effect on simulated carbon fluxes. The SiBCASA model was developed by Schaefer et al. (2008). Through a comparison with unique in situ SM observations, van der Molen et al. (2016) showed that the passive microwave SM product (AMSR-E) did not improve the SM simulated by SiBCASA, but the active microwave data, such as those from ASCAT, seem promising in some aspects. Thus, SM data obtained using ASCAT can improve the assessed spatial variation of net carbon. Hence, active microwave measurements can be useful for detecting SM beneath the forest canopy.

To overcome the shortcomings of satellite-retrieved surface SM data, Ford et al. (2014) used cross-correlation analysis to quantify the association between near-surface and root zone SM using in situ data from the United States Great Plains. The authors demonstrated that there was generally a strong relationship between near-surface and root zone SM. An exponential decay filter was used to estimate root zone soil moisture using near-surface soil moisture derived from the SMOS satellite. Root zone soil moisture derived from SMOS surface retrievals was compared to in situ soil moisture observations in the United States. Overall, the authors showed a useful approach for estimating root zone soil moisture from SMOS surface retrievals.

11.3.4 Perspectives on SM Remote Sensing

Operational SM data obtained using radiometers and scatterometers cover the past several years. However, these SM data have relatively low spatial resolutions of 25–50 km. Therefore, subpixel variations in SM can be affected by the SW fraction in the northern regions (Hogstrom and Bartsch 2016) because the pixel-wise microwave data for SM can be contaminated with SW coverage. Thus, such sub-grid scale distribution of SW causes uncertainty in SM products.

To obtain more reliable SM retrievals, fusion techniques that use data from multiple satellites are becoming important (Petropoulos et al. 2015). In the near future, this family of techniques will overcome the problems (such as low spatial resolution) associated with presently available datasets. To improve the spatial resolution of the ~40-km resolution passive microwave-derived SM, Merlin et al. (2010) used a methodology based on 1-km resolution MODIS red, near-infrared, and thermal-infrared data. The three components of this method were (1) fractional vegetation cover, (2) soil evaporative efficiency, and (3) a downscaling relationship. Airborne L-band data collected over an Australian agricultural area were used to both generate ~40-km resolution microwave pixels and verify the disaggregation results at a 4-km resolution. Among 36 different disaggregation algorithms, one was identified as being more robust. Further advancement of multi-satellite fusion and downscaling methods will improve SM estimates within eastern Siberia.

11.4 Snow

11.4.1 Remote Sensing of Snow

Snow is one of the dominant forms of water in Siberia during winter (Suzuki 2011); water from snowmelt is important for vegetation growth and water resources in eastern Siberia. Therefore, it is important to estimate the mass of snow in this region. To carry out this task, remote sensing techniques are very useful in capturing the large-scale distribution of snow, which can be detected by both optical and microwave sensor onboard satellites.

Optical sensors, such as MODIS and the National Oceanic and Atmospheric Administration (NOAA) Advanced Very High-Resolution Radiometer (AVHRR), were used to estimate fractional snow coverage at fine spatial scales; however, this method is not available when the sky is cloudy, at night, or during the polar night. Passive microwave sensors such as radiometers (SSM/I and AMSR2) are useful under cloudy conditions or in the absence of solar radiation. Although the spatial resolution of these sensors is low, their observation frequency is high (typically 1–3 days).

In this section, we describe the available snow retrieval datasets as well as the scientific results obtained using remote sensing-retrieved snow data in eastern Siberia.

11.4.2 Snow Datasets

The available snow datasets and the methods used to produce them were reviewed by Dietz et al. (2012). Consulting the study by Dietz et al. (2012), we will compile the snow datasets for eastern Siberia. In this section, we first focus on snow coverage datasets obtained using visible wavelength data, such as those obtained from MODIS and the Interactive Multisensor Snow and Ice Mapping System (IMS) instruments. Moreover, we introduce the SWE datasets obtained using the Special Sensor Microwave/Imager (SSM/I) and AMSR2 microwave sensors.

11.4.2.1 Snow Coverage Area

11.4.2.1.1 MODIS

MODIS snow products can be obtained from NASA. MODIS uses a sensor that detects in the visible wavelengths to estimate snow coverage area. MODIS snow products include two types of snow coverage area products, namely, binary snow coverage and fractional snow coverage.

Binary Snow Coverage Method (Hall and Riggs 2007; Hall et al. 2002)

The normalized difference snow index (NDSI) is used to divide regions into snow-covered and non-snow-covered areas and can be written as:

$$\left. \begin{aligned} \text{NDSI} &= \frac{\rho_4 - \rho_6}{\rho_4 + \rho_6} \\ \text{Threshold value when exists NDSI} &\geq 0.4, \\ \text{and } \rho_2 &> 0.11 \\ &\rho_4 < 0.10 \end{aligned} \right\} \quad (11.2)$$

where ρ is the surface reflectance in each band and the subscripts denote MODIS band numbers. MODIS instruments acquire data at three spatial resolutions, depending on the band. Bands 1–2 have a spatial resolution of 250 m, bands 3–7 are 500 m, and bands 8–36 are 1000 m. The wavelength ranges of band 2, band 4, and band 6 are 841–876 nm, 545–565 nm, and 1628–1652 nm, respectively.

The MODIS snow product was adjusted based on coverage by dense vegetation such as forests. If the NDVI $\cong 0.1$, the pixel may be mapped as snow even if the NDSI < 0.40 . MODIS binary snow cover products typically underestimate low-elevation snow cover by $\sim 12\%$ and typically overestimate high-elevation snow cover by $\sim 15\%$ (Klein and Barnett 2003; Parajka and Bloschl 2008).

Fractional Snow Coverage Method (Painter et al. 2003, 2009)

Fractional snow coverage is estimated using the multiple-end-member method for determining fractional snow cover and grain size.

11.4.2.1.2 IMS (Interactive Multisensor Snow and Ice Mapping System)

In addition to the MODIS snow coverage area data, a daily visual analysis of satellite data is carried out by analysts who are experienced in interpreting IMS data (Ramsay 1998). This dataset is coarser than the MODIS snow coverage area dataset. By primarily using satellite data covering the visible portion of the electromagnetic spectrum, maps of snow cover (for land areas) and sea ice cover (for ocean surface areas) are generated on a grid with a 4-km resolution. The satellite data used originate from polar orbiting satellites, e.g., AVHRR and MODIS, as well as geostationary satellites, e.g., GOES and European Union meteorological satellite (METEOSAT). Gaps due to cloud coverage and/or the absence of daylight are filled by including assessments of snow cover using passive microwave satellite data; in addition, the persistence of the snow cover is considered.

11.4.2.1.3 NOAA Weekly Data

The weekly Northern Hemisphere SCE (snow cover extent) Climate Data Record (Brown and Robinson 2011) spans the period from late 1966 to the present, comprising the longest satellite-based climate data record of any environmental variable. This CDR combines the NOAA visible satellite-based SCE analyses generated weekly through May 1999 and daily since June 1999 to form a continuous Northern Hemisphere record. The resulting continental SCE product informs climate studies, climate change monitoring, and climate model validation. The data are available from <https://www.ncdc.noaa.gov/cdr/terrestrial/snow-cover-extent-northern-hemisphere>.

11.4.2.2 Snow Water Equivalent (SWE)

11.4.2.2.1 Passive Microwave Instruments (SSM/I and AMSR2) (Foster et al. 2005; Tedesco and Jeyaratnam 2016)

This method uses a linear relationship between the differences between the 19 and 37 GHz brightness temperatures and SWE. Forest canopies disturb this relationship, and their effect on SWE estimates must be taken into account. Derksen (2008) showed that AMSR-E brightness temperature has highlighted the problematic dependence of 36.5 GHz measurements on vegetation, which can render relationships with SWE as spurious, and the differences between the 18.7 and 10.7 GHz brightness temperatures displayed a stronger correlation with SWE in boreal forest regions of Canada than the differences between the 19 and 37 GHz brightness temperatures. AMSR2 SWE datasets are available as the New LANCE NRT AMSR2 Daily L3 Global Snow Water Equivalent EASE-Grids dataset, which can be found online at <https://ghrc.nsstc.nasa.gov/home/content/new-lance-nrt-amr2-daily-l3-global-snow-water-equivalent-ease-grids-data-set-available>.

11.4.2.2.2 GlobSnow, European Space Agency (ESA)

This dataset includes SWE and snow coverage area data (Takala et al. 2011). To estimate SWE, an emission model is used to obtain snow depth from brightness temperatures for grid cells co-located with weather stations. The observed snow density values are finally used to convert snow depths into SWE. Access to this dataset is restricted, and the data provider must be contacted for their usage.

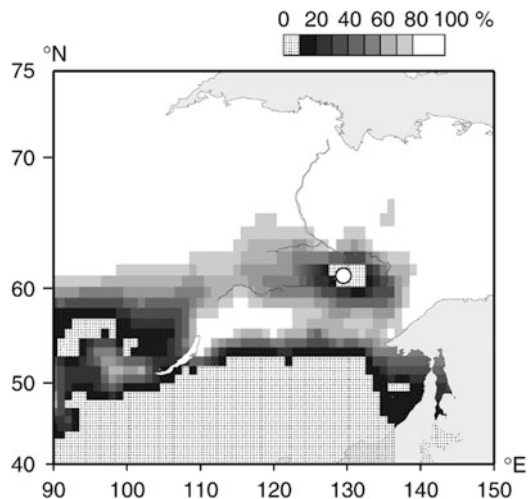
11.4.3 Scientific Applications of Snow

Here, we introduce studies using each of the different snow products. Initially, Yang et al. (2007) used snow coverage area and SWE datasets to understand the hydrological cycle in large Siberian river basins. The SWE data aid in developing an understanding of runoff generation from snowmelt in these large river basins.

Next, in terms of SCE products, using the weekly Northern Hemisphere SCE Climate Data Record, as shown in Fig. 11.2., Iijima et al. (2007) showed that the increase in air temperature and water vapor that accompanies the melting of snow was due to the advection of wet, warm air, and enhanced water vapor convergence over the central Lena River basin during the 30-day period prior to snow disappearance.

Finally, snow coverage area products can be used for model validation because of their high reliability. For instance, Suzuki et al. (2015) simulated the fine-scale distribution of snow in the Lena River basin and verified this distribution using snow coverage area data. Other climate models have used snow coverage area datasets for validation purposes (Nitta et al. 2014),

Fig. 11.2 Fifteen-year (1986–2000) composite of the ratio of snow cover existing during the week of snow disappearance in the central Lena River basin (60°N , 130°E) using NESDIS data. Reproduced from Figure 3 in (Iijima et al. 2007)



particularly the ESA GlobSnow dataset. Thus, snow retrievals by remote sensing techniques are important in the development and validation of large- or global-scale models.

11.4.4 Perspectives on Snow Remote Sensing

Snow coverage area products, especially fractional snow coverage datasets, are highly reliable and are used for model validation and many other types of studies. However, cloud and forest coverage still present many problems for performing snow retrievals. Further development of sensors for remote sensing and of more reliable retrieval algorithms is required. For instance, SWE products are less reliable in boreal forests and tundra regions. Thus, SWE products must be further developed before they can be used for research in eastern Siberia. Additionally, snow coverage area products are not reliable in areas with dense forest cover. Thus, caution is advised when applying snow coverage area products to the dense forest areas of eastern Siberia.

11.5 Surface Water (SW)

11.5.1 Remote Sensing of SW

SW is an important water resource because it can be easily used for multiple purposes, for example, as drinking water and in industrial processes. Therefore, determining the distribution of SW in eastern Siberia is critical. In addition, Huntington (2006) demonstrated that the Earth's hydrological cycle has intensified in several ways. SW is a key indicator of local and global hydrological cycles. In this section, we will describe several remote sensing techniques for assessing SW and their applications in scientific research. SW is composed of inundated areas such as lakes, ponds, and wetlands. We also introduce the major techniques for performing SW retrievals using optical sensors, passive microwave sensors, and multiple sensors and their application to scientific research in eastern Siberia.

11.5.2 SW Datasets

Here, we describe the SW retrievals performed using different sensors.

11.5.2.1 Landsat-TM

Two major products based on Landsat-TM data have been released recently. A high-resolution dataset describing lake density (the proportion of land covered by lakes) was established by Paltan et al. (2015), who used a density-slicing technique to define lake density using the shortwave infrared band 5 (1.55–1.75 μm). An SW fraction dataset with a spatial resolution of 30–90 m was constructed by Yamazaki et al. (2015) and Pekel et al. (2016), who used the normalized difference water index (NDWI: Xu 2006) and incorporated vegetation effects using NDVI data. The major difference in the products obtained by Yamazaki et al. (2015) and Pekel et al. (2016) resulted from the number of Landsat-TM images used: Yamazaki et al. (2015) used 30,000 images, whereas Pekel et al. (2016) used more than 3,000,000 images. Thus, the temporally resolved fractional SW dataset produced by Pekel et al. (2016) is more reliable than that of Yamazaki et al. (2015). The SW data (the Global 3 arc-second Water Body Map) by Yamazaki et al. (2015) can be found at http://hydro.iis.u-tokyo.ac.jp/~yamada/G3_WBM/index.html. The dataset produced by Pekel et al. (2016) is located at <https://global-surface-water.appspot.com/>.

11.5.2.2 AMSR-E/AMSR2

Passive microwave sensors were used to derive the fractional open water cover (Fw) (Watts et al. 2012) using brightness temperatures measured at 18.7 and 23.8 GHz. The data required to produce this product are more frequently available because they are collected twice daily, but the spatial resolution is 0.25°. These data can be found at https://daac.ornl.gov/cgi-bin/dsviewer.pl?ds_id=1362.

11.5.2.3 Multiple Sensors

Prigent et al. (2007) developed the first global SW dataset that reported monthly mean inundation extent using passive microwave emissivity (as measured by the SSM/I), active microwave backscattering coefficients (as determined from ERS observations), and NDVI (as determined from AVHRR observations). The spatial resolution of this dataset is 0.25°, but its temporal resolution is only monthly. The fraction of SW coverage was also reported in the dataset. The benefit of using these data is that they represent a long-term SW record for use in climate studies. This dataset is located at <https://lerma.obs-pm.fr/spip.php?article91&lang=en>.

11.5.3 Scientific Applications of SW

Understanding the carbon balance in the Arctic is important because the Arctic permafrost represents a large carbon pool. Warming and thawing of this permafrost

will cause the carbon within the permafrost to be released as carbon dioxide or methane. SW area is very important in determining methane fluxes from the Arctic. Thus, Watts et al. (2014) estimated methane fluxes using the Fw data.

The hydrological cycle in large Arctic rivers in eastern Siberia is related to SW extent. Papa et al. (2008) showed the relationships between inundation area and runoff in the three largest Siberian rivers. In the case of the Lena River, there is a clear linear relationship between SW area and runoff. However, two distinct cases exist, namely, the spring runoff and summer-to-autumn phases.

Next, we show the SW distribution around Yakutsk region in the Lena River watershed. Figure 11.3 shows the spatial distribution of water body fraction over 30 years as determined by Pekel et al. (2016). The percentage of water bodies in this area is 5.7%, and there are clearly many temporary water bodies around Yakutsk in eastern Siberia. When the SW data of Yamazaki et al. (2015) is used, the percentage of water bodies is approximately 4.0% in the area. This discrepancy occurs because Pekel et al. (2016) used 100 times more Landsat-TM data than Yamazaki et al. (2015) and estimated temporary water bodies more accurately. Therefore, the dataset provided by Pekel et al. (2016) is suitable for analyzing temporal changes in SW in eastern Siberia.

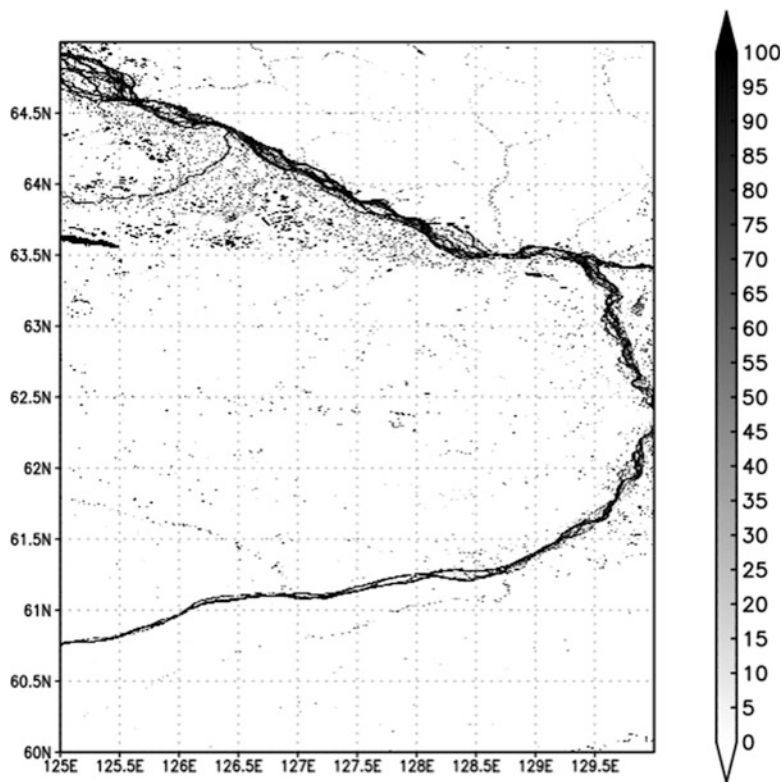


Fig. 11.3 Spatial distribution of water body fraction averaged over 30 years, estimated using the data of (Pekel et al. 2016) around Yakutsk in eastern Siberia

11.5.4 Perspectives on SW Remote Sensing

SW is a very important component of terrestrial water, both for the climate system and because its accessibility makes it convenient for usage for humans. Fine-scale spatially resolved SW data are now available, and long-term SW datasets have been developed using remote sensing techniques. To characterize the water and carbon cycles in eastern Siberia, SW retrievals can be used in many ways. Further development of SW retrieval methods will contribute to an improved understanding of the water and carbon dynamics in eastern Siberia.

11.6 Emerging Research: Data Assimilation

In this chapter, recently developed remote sensing techniques, which are used to derive TW components such as TWS, SM, snow, and SW, are reviewed. Ground-based observations neglect vast areas within eastern Siberia as accessibility is limited, and ground-based observations are too expensive. By contrast, satellite data are useful for observing TW over this large area. However, many issues must be resolved in order to enhance the accuracy of satellite retrievals.

Land surface data assimilation uses land surface models and satellite measurements. Thus, it is becoming popular because this method can fill the gaps in current satellite-based datasets. For example, each component of TW has been studied—specifically, TWS (Kumar et al. 2016), SM (Reichle et al. 2007), snow (Che et al. 2014), and SW (Revilla-Romero et al. 2016). These types of land surface data assimilation products are increasing in number, with rising applications.

The next step will involve coupled atmosphere and land surface data assimilation. This method will yield various benefits, including improved estimation of both the state of the atmosphere and TW at ground level. Such coupled atmosphere-land surface data assimilation studies are emerging in the field (Rasmy et al. 2012; Suzuki et al. 2017).

11.7 Concluding Remarks

Figure 11.4 shows a schematic of remote sensing techniques for performing TW retrievals. Only gravimetric observations can provide estimates of TWS. Optical sensors primarily detect snow and SW; passive microwave sensors primarily detect SM, snow, and SW; and active microwave sensors are mainly used to estimate SM. Passive microwave sensors provide the finest temporal resolution, followed by active microwave sensors, with optical sensors exhibiting the coarsest temporal resolution. However, in terms of spatial resolution, the ordering of the sensor

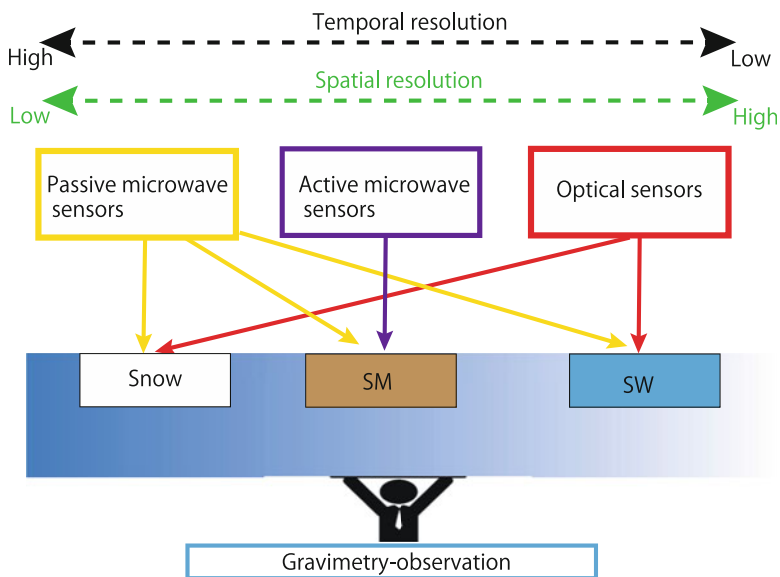


Fig. 11.4 Schematic diagram of remote sensing sensors in relation to each TW component. Solid lines (yellow, purple, red and light blue lines) indicate direct and indirect methods for estimating each TW component, respectively

types is reversed. The fusion of data from multiple satellites will produce better results than single sensors because each sensor has comparative advantages and disadvantages, and therefore, the use of fusion techniques can compensate for the drawbacks of each.

TW data can be used for a wide variety of studies, including those that address hydrology and the carbon cycle. Techniques for the remote sensing of TW are still advancing, and the development of data products depends on international satellite missions. To validate the accuracy of remote sensing retrievals, producing ground-based in situ validation data is necessary. Emerging data assimilation methods will fill the gaps between the demands of users and the shortage of remote sensing retrievals.

References

- Bartsch A, Balzter H, George C (2009) The influence of regional surface soil moisture anomalies on forest fires in Siberia observed from satellites. *Environ Res Lett* 4(4). <https://doi.org/10.1088/1748-9326/4/4/045021>
- Bettadpur S (2012) Gravity recovery and climate experiment UTSR Level-2 Processing Standards Document (Rev 4.0 May 29, 2012) (For Level-2 Product Release 0005). ftp://podaac.jpl.nasa.gov/allData/grace/docs/L2-CSR0005_ProcStd_v4.0.pdf

- Brown RD, Robinson DA (2011) Northern hemisphere spring snow cover variability and change over 1922–2010 including an assessment of uncertainty. *Cryosphere* 5(1):219–229. <https://doi.org/10.5194/tc-5-219-2011>
- Che T, Li X, Jin R, Huang C (2014) Assimilating passive microwave remote sensing data into a land surface model to improve the estimation of snow depth. *Remote Sens Environ* 143 (C):54–63. <https://doi.org/10.1016/j.rse.2013.12.009>
- Derksen C (2008) The contribution of AMSR-E 18.7 and 10.7 GHz measurements to improved boreal forest snow water equivalent retrievals. *Remote Sens Environ* 112(5):2701–2710. <https://doi.org/10.1016/j.rse.2008.01.001>
- Dietz AJ, Kuenzer C, Gessner U, Dech S (2012) Remote sensing of snow – a review of available methods. *Int J Remote Sens* 33(13):4094–4134. <https://doi.org/10.1080/01431161.2011.640964>
- Dudarev AA, Dushkina EV, Sladkova YN, Alloyarov PR, Chupakhin VS, Dorofeyev VM et al (2013) Food and water security issues in Russia II: water security in general population of Russian Arctic, Siberia and Far East, 2000–2011. *Int J Circumpolar Health* 72(0):1–11. <https://doi.org/10.3402/ijch.v72i0.22646>
- Earl L, Gardner A (2016) A satellite-derived glacier inventory for North Asia. *Ann Glaciol* 57 (71):50–60. <https://doi.org/10.3189/2016AoG71A008>
- Entekhabi D, Njoku EG, O'Neill PE, Kellogg KH, Crow WT, Edelstein WN et al (2010) The soil moisture active passive (SMAP) mission. *Proc IEEE* 98(5):704–716. <https://doi.org/10.1109/JPROC.2010.2043918>
- Figa-Saldaña J, Wilson JJW, Attema E, Gelsthorpe R, Drinkwater MR, Stoffelen A (2002) The advanced scatterometer (ASCAT) on the meteorological operational (MetOp) platform: a follow on for European wind scatterometers. *Can J Remote Sens* 28(3):404–412. <https://doi.org/10.5589/m02-035>
- Ford TW, Harris E, Quiring SM (2014) Estimating root zone soil moisture using near-surface observations from SMOS. *Hydrol Earth Syst Sci* 18(1):139–154. <https://doi.org/10.5194/hess-18-139-2014>
- Foster JL, Sun C, Walker JP, Kelly R, Chang A, Dong J et al (2005) Quantifying the uncertainty in passive microwave snow water equivalent observations. *Remote Sens Environ* 94(2):17–17. <https://doi.org/10.1016/j.rse.2004.09.012>
- Geruo A, Wahr J, Zhong S (2013) Computations of the viscoelastic response of a 3-D compressible earth to surface loading: an application to glacial isostatic adjustment in Antarctica and Canada. *Geophys J Int* 192(2):557–572. <https://doi.org/10.1093/gji/ggs030>
- Geruo A, Velicogna I, Kimball JS, Kim Y (2015) Impact of changes in GRACE derived terrestrial water storage on vegetation growth in Eurasia. *Environ Res Lett* 10(12):1–10. <https://doi.org/10.1088/1748-9326/10/12/124024>
- Hall DK, Riggs GA (2007) Accuracy assessment of the MODIS snow products. *Hydrol Process* 21 (12):1534–1547. <https://doi.org/10.1002/hyp.6715>
- Hall DK, Kelly R, Riggs GA, Chang A, Foster JL (2002) Assessment of the relative accuracy of hemispheric-scale snow-cover maps. *Ann Glaciol* 34(1):24–30. <https://doi.org/10.3189/172756402781817770>
- Hogstrom E, Bartsch A (2016) Impact of backscatter variations over water bodies on coarse-scale radar retrieved soil moisture and the potential of correcting with meteorological data. *IEEE Trans Geosci Remote Sens* 55(1):3–13. <https://doi.org/10.1109/TGRS.2016.2530845>
- Hood JL, Hayashi M (2015) Characterization of snowmelt flux and groundwater storage in an alpine headwater basin. *J Hydrol* 521:482–497
- Huntington TG (2006) Evidence for intensification of the global water cycle: review and synthesis. *J Hydrol* 319(1–4):83–95
- Iijima Y, Masuda K, Ohata T (2007) Snow disappearance in eastern Siberia and its relationship to atmospheric influences. *Int J Climatol* 27(2):169–177. <https://doi.org/10.1002/joc.1382>

- Imaoka K, Kachi M, Fujii H, Murakami H, Hori M, Ono A, Igarashi T, Nakagawa K, Oki T, Honda Y, Shimoda H (2010) Global Change Observation Mission (GCOM) for monitoring carbon, water cycles, and climate change. *Proc IEEE* 98(5):717–734
- Kachi M, Maeda T, Tsutsui H, Imaoka K (2015) The water-related parameters and datasets derived from GCOM-W/AMSR2. IGARSS. <https://doi.org/10.1109/IGARSS.2015.7326979>
- Keiji Imaoka, Misako Kachi, Hideyuki Fujii, Hiroshi Murakami, Masahiro Hori, Akiko Ono, Tamotsu Igarashi, Keizo Nakagawa, Taikan Oki, Yoshiaki Honda, Haruhisa Shimoda, Global Change Observation Mission (GCOM) for Monitoring Carbon, Water Cycles, and Climate Change. *Proceedings of the IEEE* 98 (5):717-734
- Kerr YH, Waldteufel P, Wigneron J-P, Delwart S, Cabot F, Boutin J et al (2010) The SMOS mission – new tool for monitoring key elements of the global water cycle. *Proc IEEE* 98 (5):666–687. <https://doi.org/10.1109/JPROC.2010.2043032>
- Klein AG, Barnett AC (2003) Validation of daily MODIS snow cover maps of the upper Rio Grande River basin for the 2000-2001 snow year. *Remote Sens Environ* 86(2):162–176. [https://doi.org/10.1016/S0034-4257\(03\)00097-X](https://doi.org/10.1016/S0034-4257(03)00097-X)
- Kumar SV, Zaitchik BF, Peters-Lidard CD, Rodell M, Reichle R, Li B et al (2016) Assimilation of gridded GRACE terrestrial water storage estimates in the north American land data assimilation system. *J Hydrometeorol* 17(7):1951–1972. <https://doi.org/10.1175/JHM-D-15-0157.1>
- Kusche J (2007) Approximate decorrelation and non-isotropic smoothing of time-variable GRACE-type gravity field models. *J Geod* 81(11):733–749. <https://doi.org/10.1007/s00190-007-0143-3>
- Masuda K, Hashimoto Y, Matsuyama H, Oki T (2001) Seasonal cycle of water storage in major river basins of the world. *Geophys Res Lett* 28(16):3215–3218. <https://doi.org/10.1029/2000GL012444>
- Merlin O, Bitar Al A, Walker JP, Kerr Y (2010) An improved algorithm for disaggregating microwave-derived soil moisture based on red, near-infrared and thermal-infrared data. *Remote Sens Environ* 114(10):2305–2316. <https://doi.org/10.1016/j.rse.2010.05.007>
- Muskett RR, Romanovsky VE (2009) Groundwater storage changes in arctic permafrost watersheds from GRACE and in situ measurements. *Environ Res Lett* 4(4):045009. <https://doi.org/10.1088/1748-9326/4/4/045009>
- Nitta T, Yoshimura K, Takata K, O’ishi R, Sueyoshi T, Kanae S et al (2014) Representing variability in subgrid snow cover and snow depth in a global land model: offline validation. *J Clim* 27:3318–3330. <https://doi.org/10.1175/JCLI-D-13-00310.1>
- Owe M, de Jeu R, Holmes T (2008) Multisensor historical climatology of satellite-derived global land surface moisture. *J Geophysical Res* 113(F1):687–617. <https://doi.org/10.1029/2007JF000769>
- Painter TH, Dozier J, Roberts DA, Davis RE, Green RO (2003) Retrieval of subpixel snow-covered area and grain size from imaging spectrometer data. *Remote Sens Environ* 85(1):64–77. [https://doi.org/10.1016/S0034-4257\(02\)00187-6](https://doi.org/10.1016/S0034-4257(02)00187-6)
- Painter TH, Rittger K, McKenzie C, Slaughter P, Davis RE, Dozier J (2009) Retrieval of subpixel snow covered area, grain size, and albedo from MODIS. *Remote Sens Environ* 113(4):868–879. <https://doi.org/10.1016/j.rse.2009.01.001>
- Paltan H, Dash J, Edwards M (2015) A refined mapping of Arctic lakes using Landsat imagery. *Int J Remote Sens* 36(23):5970–5982. <https://doi.org/10.1080/01431161.2015.1110263>
- Papa F, Prigent C, Rossow WB (2008) Monitoring flood and discharge variations in the large Siberian rivers from a multi-satellite technique. *Surv Geophys* 29(4–5):297–317. <https://doi.org/10.1007/s10712-008-9036-0>
- Parajka J, Blöschl G (2008) Spatio-temporal combination of MODIS images – potential for snow cover mapping. *Water Resour Res* 44(3). <https://doi.org/10.1029/2007WR006204>
- Pekel J-F, Cottam A, Gorelick N, Belward AS (2016) High-resolution mapping of global surface water and its long-term changes. *Nature* 540(7633):418–422. <https://doi.org/10.1038/nature20584>

- Petropoulos GP, Ireland G, Barrett B (2015) Surface soil moisture retrievals from remote sensing: current status, products & future trends. *Phys Chem Earth* 83–84:36–56. <https://doi.org/10.1016/j.pce.2015.02.009>
- Prigent C, Papa F, Aires F, Rossow WB, Matthews E (2007) Global inundation dynamics inferred from multiple satellite observations, 1993–2000. *J Geophys Res* 112(D12):D12107–D12113. <https://doi.org/10.1029/2006JD007847>
- Quinton WL, Hayashi M, Pietroniro A (2003) Connectivity and storage functions of channel fens and flat bogs in northern basins. *Hydrol Process* 17(18):3665–3684
- Ramsay BH (1998) The interactive multisensor snow and ice mapping system. *Hydrol Process* 12(1):1537–1546. [https://doi.org/10.1002/\(SICI\)1099-1085\(199808/09\)12:10/11<1537::AID-HYP679>3.3.CO;2-1](https://doi.org/10.1002/(SICI)1099-1085(199808/09)12:10/11<1537::AID-HYP679>3.3.CO;2-1)
- Rasmy M, Koike T, Kuria D, Mirza CR, Li X, Yang K (2012) Development of the coupled atmosphere and land data assimilation system (CALDAS) and its application over the Tibetan plateau. *IEEE Trans Geosci Remote Sens* 50(11):4227–4242. <https://doi.org/10.1109/TGRS.2012.2190517>
- Reichle RH, Koster RD, Liu P, Mahanama SPP, Njoku EG, Owe M (2007) Comparison and assimilation of global soil moisture retrievals from The Advanced Microwave Scanning Radiometer For the Earth Observing System (AMSR-E) and the Scanning Multichannel Microwave Radiometer (SMMR). *J Geophys Res Atmos* 112(D):D09108. <https://doi.org/10.1029/2006JD008033>
- Revilla-Romero B, Wanders N, Burek P, Salamon P, de Roo A (2016) Integrating remotely sensed surface water extent into continental scale hydrology. *J Hydrol* 543(Part B):659–670. <https://doi.org/10.1016/j.jhydrol.2016.10.041>
- Schaefer K, Collatz GJ, Tans P, Denning AS, Baker I, Berry J, Prihodko L, Suits N, Philpott A (2008) Combined simple biosphere/carnegie-Ames-Stanford approach terrestrial carbon cycle model. *J Geophys Res Biogeo* 113:G03034. <https://doi.org/10.1029/2007jg000603>
- Seo K-W, Ryu D, Kim B-M, Waliser DE, Tian B, Eom J (2010) GRACE and AMSR-E-based estimates of winter season solid precipitation accumulation in the Arctic drainage region. *J Geophys Res* 115(D20):D20117–D20118. <https://doi.org/10.1029/2009JD013504>
- Sugimoto A, Naito D, Yanagisawa N, Ichiyonagi K, Kurita N, Kubota J et al (2003) Characteristics of soil moisture in permafrost observed in east Siberian taiga with stable isotopes of water. *Hydrol Process* 17(6):1073–1092. <https://doi.org/10.1002/hyp.1180>
- Suzuki K (2011) Siberia. In: *Encyclopedia of snow, ice and glaciers*. Springer Netherlands, Dordrecht, pp 1028–1031. https://doi.org/10.1007/978-90-481-2642-2_486
- Suzuki K, Kubota J, Ohata T, Vuglinsky V (2006) Influence of snow ablation and frozen ground on spring runoff generation in the Mogot experimental watershed, southern mountainous taiga of eastern Siberia. *Hydrol Res* 37(1):21–29. <https://doi.org/10.2166/nh.2005.027>
- Suzuki K, Liston GE, Matsuo K (2015) Estimation of continental-basin-scale sublimation in the Lena River Basin, Siberia. *Adv Meteorol* 2015(22):1–14. <https://doi.org/10.1155/2015/286206>
- Suzuki K, Matsuo K, Hiyama T (2016) Satellite gravimetry-based analysis of terrestrial water storage and its relationship with run-off from the Lena River in eastern Siberia. In *J Remote Sens* 37(10):2198–2210. <https://doi.org/10.1080/01431161.2016.1165890>
- Suzuki K, Zupanski M, Zupanski D (2017) A case study involving single observation experiments performed over snowy Siberia using a coupled atmosphere-land modelling system. *Atmos Sci Lett* 18(3):106–111. <https://doi.org/10.1002/asl.730>
- Suzuki K, Matsuo K, Yamazaki D, Ichii K, Iijima Y, Yanagi Y et al (2018) Hydrological variability and changes in the Arctic circumpolar tundra and the three largest pan-Arctic river basins from 2002 to 2016. *Remote Sens* 2018(10):402. <https://doi.org/10.3390/rs10030402>
- Swenson S, Wahr J (2006) Post-processing removal of correlated errors in GRACE data. *Geophys Res Lett* 33(8):L08402–4. <https://doi.org/10.1029/2005GL025285>
- Takala M, Luojus K, Pulliainen J, Derksen C, Lemmetyinen J, Kämä J-P et al (2011) Estimating northern hemisphere snow water equivalent for climate research through assimilation of space-

- borne radiometer data and ground-based measurements. *Remote Sens Environ* 115 (12):3517–3529. <https://doi.org/10.1016/j.rse.2011.08.014>
- Tapley BD, Bettadpur S, Ries JC, Thompson PF, Watkins MM (2004) GRACE measurements of mass variability in the Earth system. *Science* 305(5683):503–505. <https://doi.org/10.1126/science.1099192>
- Tedesco M, Jeyaratnam J (2016) A new operational snow retrieval algorithm applied to historical AMSR-E brightness temperatures. *Remote Sens* 8(12):1037. <https://doi.org/10.3390/rs8121037>
- van der Molen MK, de Jeu RAM, Wagner W, van der Velde IR, Kolari P, Kurbatova J et al (2016) The effect of assimilating satellite-derived soil moisture data in SiBCASA on simulated carbon fluxes in Boreal Eurasia. *Hydrol Earth Syst Sci* 20(2):605–624. <https://doi.org/10.5194/hess-20-605-2016>
- Velicogna I, Tong J, Zhang T, Kimball JS (2012) Increasing subsurface water storage in discontinuous permafrost areas of the Lena River basin, Eurasia, detected from GRACE. *Geophys Res Lett* 39(9):L09403. <https://doi.org/10.1029/2012GL051623>
- Vey S, Steffen H, Müller J, Boike J (2013) Inter-annual water mass variations from GRACE in Central Siberia. *J Geod* 87(3):287–299. <https://doi.org/10.1007/s00190-012-0597-9>
- Wagner W, Hahn S, Kidd R, Melzer T, Bartalis Z, Hasenauer S et al (2013) The ASCAT soil moisture product: a review of its specifications, validation results, and emerging applications. *Meteorol Z* 22(1):5–33. <https://doi.org/10.1127/0941-2948/2013/0399>
- Wahr J, Molenaar M, Bryan F (1998) Time variability of the Earth's gravity field: hydrological and oceanic effects and their possible detection using GRACE. *J Geophys Res* 103 (B12):30205–30229. <https://doi.org/10.1029/98JB02844>
- Wahr J, Swenson S, Zlotnicki V, Velicogna I (2004) Time-variable gravity from GRACE: first results. *Geophys Res Lett* 31(11). <https://doi.org/10.1029/2004GL019779>
- Watts JD, Kimball JS, Jones LA, Schroeder R, McDonald KC (2012) Satellite microwave remote sensing of contrasting surface water inundation changes within the Arctic–Boreal region. *Remote Sens Environ* 127:223–236. <https://doi.org/10.1016/j.rse.2012.09.003>
- Watts JD, Kimball JS, Bartsch A, McDonald KC (2014) Surface water inundation in the boreal-Arctic: potential impacts on regional methane emissions. *Environ Res Lett* 9(7):075001. <https://doi.org/10.1088/1748-9326/9/7/075001>
- Xu H (2006) Modification of normalised difference water index (NDWI) to enhance open water features in remotely sensed imagery. *Int J Remote Sens* 27(14):3025–3033. <https://doi.org/10.1080/01431160600589179>
- Yamazaki D, Trigg MA, Ikeshima D (2015) Development of a global ~90 m water body map using multi-temporal Landsat images. *Remote Sens Environ* 171(C):337–351. <https://doi.org/10.1016/j.rse.2015.10.014>
- Yang D, Zhao Y, Armstrong R, Robinson D, Brodzik M-J (2007) Streamflow response to seasonal snow cover mass changes over large Siberian watersheds. *J Geophys Res Earth Surf* 112(F): F02S22. <https://doi.org/10.1029/2006JF000518>